AIAA SciTech Forum
8-12 January 2024, Orlando, FL
AIAA SCITECH 2024 Forum

10.2514/6.2024-1873

Indirect Optimal Control Techniques for Multimode Propulsion Mission Design

Bryan C. Cline, * Alex Pascarella, † Robyn M. Woollands,‡ and Joshua L. Rovey§
University of Illinois Urbana-Champaign, Urbana, Illinois, 61801

Multimode spacecraft propulsion has the potential to greatly increase the maneuvering capability of spacecraft in comparison to traditional architectures. This technology combines two or more propulsive modes into a single system with a single propellant. Trajectory design techniques for spacecraft with this capability, however, are limited and typically require manual selection of the burn sequence. In this study, indirect optimal control formulations with automatic mode selection are developed and applied for the first time for multimode spacecraft with two modes of operation. Minimum-fuel transfers are solved in polar coordinates and Mean Equinoctial Elements. Propellant-constrained minimum-time problems are also solved for the first time using a penalty function approach. An interior-point constraint formulation is also provided. The focus of this work is the development of trajectory optimization techniques for multimode-propelled spacecraft. Sample transfers are presented for each coordinate choice and optimization objective and are compared to single mode approaches. The results demonstrate viability of the proposed techniques and show the multimode approach can reduce the time-of-flight in comparison to a low-thrust only trajectory while providing mass savings over high-thrust only solutions.

I. Introduction

Multimode spacecraft propulsion is an emerging, enabling, and enhancing technology that may greatly increase the maneuvering capability domain for spacecraft while reducing dry mass in comparison to traditional architectures [1]. This technology integrates two or more propulsion modes into a single system using a single propellant and is distinct from hybrid propulsion in which two or more modes may be present on a spacecraft but are not integrated. While there are many possible multimode systems (see Fig. 1 of Ref. [1]), systems with a high-thrust, low specific impulse mode and a low-thrust, high specific impulse mode are particularly intriguing to mission designers because of their ability to provide a wide capability domain. One of the primary challenges facing mission designers exploring the use of multimode propulsion is a lack of dedicated techniques for developing optimal multimode trajectories. As a result, mission designers are often forced to assume a sequence of burns (e.g., high-thrust followed by low-thrust) rather than determine the optimal sequence as part of the optimization process. In this study, techniques are developed for solving multimode minimum-time transfers and propellant-constrained minimum-fuel transfers. The former is solved in both polar coordinates as well as Mean Equinoctial Elements (MEEs) [2] while the latter is solved in MEEs. Here, the emphasis is on development of the techniques rather than design of specific trajectories. In all three cases, constant thruster performance was assumed (i.e., constant thrust and specific impulse). Note that while the problems formulated in this study are framed in terms of multimode propulsion, the methods naturally extend to hybrid propulsion because they are agnostic to the source of the thrust.

Minimum-fuel transfers are particularly valuable for science and exploration missions that require the delivery of the maximum payload mass. Several authors have explored the potential benefits of multimode and hybrid propulsion systems for transfers to Mars [3–9]. Benefits, including reduced trip times and reduced propellant requirements, have been shown by Gilland [3], Percy *et al.* [5], and Chai *et al.* [6, 7] for human-class missions. Mingotti *et al.* also found hybrid propulsion provides increased fuel efficiency over all-electric and all-chemical transfers to Mars [4]. Additionally, a hybrid chemical-electric propulsion system was found to be mission enabling by Mani *et al.* for a Mars CubeSat mission [8]. In this study, the new optimal control formulation, which automatically selects the burn sequence, is demonstrated using polar coordinates for a minimum-fuel transfer from Earth's orbit about the Sun to that of Mars.

*Graduate Research Assistant, Department of Aerospace Engineering, AIAA Student Member. bcline3@illinois.edu
†Graduate Research Assistant, Department of Aerospace Engineering. alexp3@illinois.edu
‡Assistant Professor, Department of Aerospace Engineering. rmw@illinois.edu
§Professor, Department of Aerospace Engineering, AIAA Associate Fellow. rovey@illinois.edu

Orbit raising is another class of missions that has been studied for multimode and hybrid propulsion. Several studies have shown significant mass savings for transfers to geosynchronous (or geostationary) orbit (GEO) using multimode or hybrid propulsion in comparison to traditional high-thrust only approaches [10–15]. An analytical method for determining the optimal intermediate orbit to begin a low-thrust burn for a transfer to GEO using chemical and electric propulsion sequentially was developed by Kluever [13]. Jenkin explored trends across a range of launch vehicle capabilities, spacecraft steering laws, and thruster power settings for minimum-fuel transfers to GEO [16]. Ceccherini *et al.* developed a method for optimizing elements of the spacecraft system design alongside the trajectory for transfers to GEO using sequential hybrid propulsion (i.e., high-thrust followed by low-thrust). Notably, the authors included the impact of the Van Allen Belts within the spacecraft optimization [17]. Other mission classes, including formation flight [18] and lunar missions [19–21], were extensively reviewed in Ref. [1]. In keeping with the focus of much of the literature, a geosynchronous transfer orbit (GTO) to GEO transfer is used in this study to demonstrate a three-dimensional, minimum-fuel problem using MEEs.

The final problem solved in this study is the propellant-constrained minimum-time (PCMT) problem for spacecraft with two modes of operation. In this problem, the objective is to reach the final orbit as quickly as possible subject to a propellant constraint on the higher thrust, lower specific impulse mode. Without this constraint, the higher thrust mode would be used to complete the entire transfer. This problem is particularly relevant for multimode spacecraft that desire fast transfers but are subject to maximum throughput or other constraints in the high-thrust mode as well as spacecraft with hybrid propulsion and fixed propellant mass budgets. The latter is reflective of commercial spacecraft operating with an existing, commercially available bus with hybrid propulsion (e.g., A2100 or LM2100) that desire reaching their revenue-generating orbit as quickly as possible to maximize profit. Additionally, this approach can be applied to trajectory redesign efforts to correct for launch injection errors, like those experienced by USA-214 (AEHF-1) and Al Yah 3, missed thrust events, or partial propulsion system failures. Solving this problem using an optimal control formulation represents an improvement over the multiple solver approach used in the Al Yah 3 rescue efforts [22].

A penalty function approach was taken to solve the PCMT problem. Penalty functions are a canonical method for enforcing equality or inequality constraints on a state or control variable in an optimal control problem [23]. Here, the penalty function is added to the cost functional to enforce an inequality constraint on the high-thrust mode propellant consumed (i.e., the propellant consumed must be less than or equal to a specified value). This approach was selected due to its ease of application within the framework developed for solving minimum-fuel problems. An alternative approach to solving this problem requires the application of an interior-point constraint (i.e., a set of boundary conditions at an interior time on the trajectory) [23]. A derivation for this method is also provided.

Broadly, there are two types of optimal control solution formulations: direct and indirect. Direct approaches transcribe an optimal control problem into a nonlinear programming problem, and the optimal solution must satisfy the Karush-Kuhn-Tucker conditions [24, 25]. Direct methods are simple to initialize but may not converge to an optimal solution [26] and are often computationally expensive [27]. Indirect approaches aim to solve a multipoint boundary value problem (i.e., two or more boundaries) by applying Pontryagin's Minimum Principle [28]. This approach requires the derivation of the costate dynamics via the Euler-Lagrange equations. The transversality conditions (boundary conditions on the costates or the Hamiltonian) must also be satisfied. Indirect approaches guarantee satisfaction of the first-order necessary conditions (n.b., the second-order necessary conditions and the sufficient conditions may or may not be satisfied), but may be difficult to solve due to the need for a suitable initial guess for the costates [26]. Approaches, including both direct and indirect methods, for solving trajectory optimization problems were reviewed in detail in Ref. [29] and, more recently, low-thrust trajectory optimization approaches were reviewed in Ref. [26]. In this study, an indirect approach was selected due to its relatively low computational expense and its guarantee that the first-order necessary conditions are satisfied.

In both minimum-fuel and minimum-time problems, a switch function can be developed that governs whether the thruster is active or inactive. Note switch functions are often neglected in canonical (single mode) minimum-time problems because the thruster is always on. In a bang-off-bang solution, the thrust value is set to its maximum when the switch function is greater than zero and set to zero when the switch function is less than zero. It is typically assumed that singular arcs (when the switch function is equal to zero for a finite duration) rarely occur in trajectories of interest. This switching behavior for the throttle is inherently non-smooth and often leads to difficulty in achieving numerical convergence. Taheri and Junkins introduced a new technique known as hyperbolic tangent smoothing that approximates the switch function with the hyperbolic tangent function and a homotopy (continuation) parameter in order to increase the domain of convergence [30]. As the homotopy parameter approaches zero, the hyperbolic tangent function approaches the bang-off-bang solution. In this study, the hyperbolic tangent smoothing technique is used to control the throttle setting of each mode and within the penalty function for the PCMT problem. To the author's

knowledge, this is the first application of hyperbolic tangent smoothing to a penalty function approach for a state variable inequality constrained problem.

Taheri *et al.* recently developed a new technique known as Composite Smooth Control (CSC). This method extends the hyperbolic tangent smoothing technique to address challenges related to nonlinear dynamics by applying a smoothing method to introduce nonlinearities into the dynamics. The authors apply hyperbolic tangent smoothing to smooth switches between operating points. This method has been demonstrated for fuel optimal transfers using variable specific impulse thrusters [31] and multiple engines [32]. The authors found good convergence properties and reasonable computational speed for the trajectories studied. Taheri has also applied CSC to multi-revolution transfers to a comet [33, 34]. Arya *et al.* applied CSC to low-thrust gravity-assist trajectory design [35] as well as to simultaneous optimization of a trajectory and a propulsion system [36]. The CSC approach has also been used to develop low-thrust trajectories subject to eclipses [37]. Note that the authors in Refs. [31–36] use "multimode" to refer to thrusters or collections of thrusters with multiple operational set points as opposed to a system with two or more integrated propulsive modes. Despite the range of applications of CSC, it presently does not address multimode systems with distinct modes that operate at the exclusion of others.

Recent work by Cline *et al.* demonstrated, for the first time, the capability of a novel multimode monopropellant-electrospray thruster for NASA-relevant lunar CubeSat missions using high-fidelity modeling. The authors assumed an 8.0 kg propellant limit and found the multimode system was able to complete three of the four design reference missions (DRM) and the fourth could be completed with a 7% increase in propellant mass while an all-chemical system could complete only two DRMs and an all-electric system could only complete three missions. The multimode system was found to complete the missions using up to 33% less propellant than the all-chemical system and in up to 55% less time than the all-electric approach [21]. These results, however, were found using point solutions rather than optimized solutions that minimize a cost functional. This emphasizes the need for a new technique to model multimode transfers.

A separate, rapidly growing branch of the literature (not reviewed exhaustively here) has explored mission design for spacecraft with electric propulsion systems that can operate at a variety of power levels. For example, Quarta and Mengali developed power-limited minimum-time trajectories to multiple planets and asteroids using a model of an ion thruster with 41 discrete operating levels (n.b., while the literature occasionally assumes performance of a thruster can vary continuously, most practical systems operate at discrete performance levels). As would be anticipated, the thruster operates at the highest thrust level possible at each stage in the trajectory to minimize the flight time [38]. Similarly, Chi *et al.* developed time-optimal and fuel-optimal trajectories to Mars using discrete operating levels of an NSTAR thruster subject to power availability [39]. Li *et al.* also compared dual specific impulse thrusters to variable specific impulse thrusters for power-limited, fuel-optimal, interplanetary transfers [40]. The aforementioned studies share a great deal in common with optimal multimode trajectory design: techniques were developed to select the optimal mode at every instant throughout the trajectory. The three investigations cited here, however, are mildly simplified in comparison to the problems studied in this investigation due to the power limitation. For the minimum-time transfers, the mode operated is typically the highest possible thrust mode. Some minor variation is seen in the minimum-fuel transfers in Ref. [39]. Nonetheless, the approaches used in these studies do not fully resolve the challenges of constant performance multimode trajectory design because the power limitation aids in the selection of the optimal operation mode.

The primary contribution of this paper is the development and detailing of new indirect optimal control techniques for multimode minimum-fuel and PCMT transfers that automatically select the burn sequence. Addressing the minimum-fuel problem aims to alleviate the limitations of approaches that require manual selection of the burn sequence as well as those that do not permit operation of a single mode at a time (e.g., Ref. [32]). The PCMT problem is seldom discussed in the literature but has near-term and long-term impact for multimode and hybrid trajectories.

The remainder of this paper is organized as follows: Section II details the methodology and formulation of the optimal control problem while Section III provides results and discusses their impact; the paper is concluded in Section IV.

II. Methodology

This section details the optimal control formulation for both the minimum-fuel and minimum-time problems investigated in this study. Indirect optimal control formulations are given in polar coordinates and MEEs for the multimode minimum-fuel problem while the PCMT problem is presented in MEEs. In all three cases, two-body dynamics were assumed. The propulsion system was assumed to have two modes of operation and have constant performance values (i.e., constant thrust and specific impulse).

A. Minimum-Fuel Problem: Polar Coordinates

The cost functional to be minimized for the minimum-fuel problem is shown in Eq. 1 in Lagrange form. Here, T_1 and T_2 are the thrust values for each mode while c_1 and c_2 are the modes' specific impulses multiplied by Earth's standard gravitational acceleration (i.e., $c_i = I_{sp_i} g_0$). The lower thrust, higher specific impulse mode is assumed to be mode 1. The throttle values are represented by δ_1 and δ_2 and take on values between 0 (fully off) and 1 (fully on). The value of this functional is the total propellant consumed.

$$J = \int_{t_0}^{t_f} \left(\frac{T_1}{c_1}\delta_1 + \frac{T_2}{c_2}\delta_2 \right) dt = \int_{t_0}^{t_f} L dt \tag{1}$$

The dynamics for this problem are given in Eq. 2 in polar coordinates. The state variables are the radial position, r, the angular position, θ, the radial velocity, u, the tangential velocity, v, and the spacecraft mass, m. The Sun's gravitational parameter is represented by μ and the components of the thrust unit vector in the radial and tangential directions are u_1 and u_2, respectively.

$$\dot{\boldsymbol{x}} = \begin{bmatrix} \dot{r} \\ \dot{\theta} \\ \dot{u} \\ \dot{v} \\ \dot{m} \end{bmatrix} = \begin{bmatrix} u \\ \frac{v}{r} \\ \frac{v^2}{r} - \frac{\mu}{r^2} + \frac{T_1}{m}\delta_1 u_1 + \frac{T_2}{m}\delta_2 u_1 \\ \frac{-uv}{r} + \frac{T_1}{m}\delta_1 u_2 + \frac{T_2}{m}\delta_2 u_2 \\ -\frac{T_1}{c_1}\delta_1 - \frac{T_2}{c_2}\delta_2 \end{bmatrix} = \boldsymbol{f} \tag{2}$$

Using the dynamics and an indirect approach, the Hamiltonian may be written as shown in Eq. 3. The costates are represented by the $\boldsymbol{\lambda}$ vector.

$$H = L + \boldsymbol{\lambda}^T \boldsymbol{f} \tag{3}$$

The optimal control for this problem must minimize the Hamiltonian per Pontryagin's Minimum Principle [28]. By applying primer vector theory [41, 42], the optimal u_1 and u_2 (indicated with a superscript *) that minimize the Hamiltonian may be found as shown in Eqs. 4 and 5.

$$u_1^* = -\frac{\lambda_u}{|| \left[\lambda_u \; \lambda_v\right] ||} \tag{4}$$

$$u_2^* = -\frac{\lambda_v}{|| \left[\lambda_u \; \lambda_v\right] ||} \tag{5}$$

In order to solve the optimal control problem numerically, it is necessary to derive the dynamics of the costates for propagation alongside the states. These time derivatives are given by the Euler-Lagrange equations, shown in Eq. 6.

$$\dot{\boldsymbol{\lambda}} = -\left[\frac{\partial H}{\partial \boldsymbol{x}}\right]^T \tag{6}$$

The switch functions that determine when each mode is active are shown in Eq. 7. These are found by collecting all terms multiplied by δ_1 and δ_2, respectively, in the Hamiltonian and reversing their sign. The sign reversal is for convenience only and ensures the mode may be active when the value of the switch function is positive.

$$S_i = -\frac{T_i}{c_i}\left(1 + \frac{c_i}{m}u_1^*\lambda_u + \frac{c_i}{m}u_2^*\lambda_v - \lambda_m\right) \tag{7}$$

The throttle value for each mode may be found as shown in Eqs. 8 and 9. These expressions make use of hyperbolic tangent smoothing, which is a homotopy approach used to aid numerical convergence by smoothing sharp changes in the system dynamics [27, 30]. Here, ρ is a homotopy parameter swept from 1 to a small, user-supplied value, typically on the order of $1 * 10^{-4}$ or smaller, to sufficiently approximate a bang-off-bang solution. Note the final value of the homotopy parameter is problem dependent and should be selected to correspond to a very small change in the final states (e.g., $< 1\%$). Singular arcs, which occur when $S = 0$ for a finite duration, do not occur on the trajectories found.

$$\delta_1 = \begin{cases} 1 & if\ S_1 > 0 \\ 0 & if\ S_1 < 0 \end{cases} = \frac{1}{2}\left(1 + \text{sgn}(S_1)\right) \approx \frac{1}{2}\left(1 + \tanh(S_1/\rho)\right) \tag{8}$$

$$\delta_2 = \begin{cases} 1 & if\ S_2 > 0 \\ 0 & if\ S_2 < 0 \end{cases} = \frac{1}{2}\left(1 + \text{sgn}(S_2)\right) \approx \frac{1}{2}\left(1 + \tanh(S_2/\rho)\right) \tag{9}$$

In this work, it is assumed only one of the two modes may be active at a time. This is typical for multimode systems that only have a single thruster head (see Ref. [21]). This is also a valid assumption for systems with vastly different levels of thrust (i.e., when a low-thrust mode would not meaningfully contribute to a high-thrust burn) or where power or other constraints may limit the use of more than one mode at a time. Equations 7-9, however, do not include this constraint. In order to apply this constraint, a Hamiltonian for both modes, H_1 and H_2, respectively, may be constructed. To do so, δ_2 is set equal to 0 in Eq. 3 to form H_1 and $\delta_1 = 0$ to form H_2. As a result, the dynamics and the thrust contributions from the relevant mode are retained. Since this problem is formulated to minimize the Hamiltonian (Eq. 3,) the mode that should be active corresponds to that with the smaller value of the mode-specific Hamiltonian (i.e., H_1 or H_2). Thus, at every instant along the trajectory, the throttles are redefined as shown in Eqs. 10-11. This approach retains the previously described hyperbolic tangent smoothing approach because the optimal throttle (i.e., the throttle that minimizes the Hamiltonian) is set either to 0 or the current value as found using Eqs. 8-9 rather than to strictly 0 or 1.

$$\delta_1^* = \begin{cases} \delta_1 & if\ H_1 \leq H_2 \\ 0 & if\ H_1 > H_2 \end{cases} \tag{10}$$

$$\delta_2^* = \begin{cases} \delta_2 & if\ H_2 < H_1 \\ 0 & if\ H_2 \geq H_1 \end{cases} \tag{11}$$

The optimal throttle values, at every instant, can then be inserted into Eq. 3 and used to update the costate dynamics (Eq. 6).

B. Minimum-Fuel Problem: MEEs

Three-dimensional, minimum-fuel trajectories were found by reformulating the minimum-fuel problem in MEEs. Using MEEs typically leads to greater convergence than Cartesian coordinates because five of the six variables are slow variables (change slowly) while Cartesian coordinates have six fast variables. They also only have a singularity at an inclination of 180° and are valid for circular, elliptical, or hyperbolic trajectories [27, 43].

The minimum-fuel cost functional remains as given in Eq. 1. The dynamics are given in Eq. 12. The state variables are p (the semilatus rectum), f, g, h, k, L (the true longitude), and the total spacecraft mass, m. See Ref. [2] for the MEEs relationship to the classical orbital elements. The $\boldsymbol{A}$ vector and $\boldsymbol{B}$ matrix are defined in Eqs. 13-14. Equations for q and s^2 are given in Eqs. 15-16 to condense the expressions in $\boldsymbol{A}$ and $\boldsymbol{B}$. Note the last element of $\boldsymbol{A}$ is the differential equation for the total mass of the spacecraft. The corresponding row of $\boldsymbol{B}$ is identically zero because this is an auxiliary equation to the traditional MEEs.

$$\dot{\boldsymbol{x}} = \boldsymbol{A} + \frac{T_1}{m}\delta_1 \boldsymbol{B}\boldsymbol{u} + \frac{T_2}{m}\delta_2 \boldsymbol{B}\boldsymbol{u} = \boldsymbol{f} \tag{12}$$

$$\boldsymbol{A} = \begin{bmatrix} 0 & 0 & 0 & 0 & 0 & \sqrt{\mu p}\left(\frac{q}{p}\right)^2 & -\left(\frac{T_1}{c_1}\delta_1 + \frac{T_2}{c_2}\delta_2\right) \end{bmatrix}^T \tag{13}$$

$$\boldsymbol{B} = \begin{bmatrix} 0 & \frac{2p}{q}\sqrt{\frac{p}{\mu}} & 0 \\ \sqrt{\frac{p}{\mu}}\sin L & \sqrt{\frac{p}{\mu}}\frac{1}{q}\left[(q+1)\cos L + f\right] & -\sqrt{\frac{p}{\mu}}\frac{g}{q}\left[h\sin L - k\cos L\right] \\ -\sqrt{\frac{p}{\mu}}\cos L & \sqrt{\frac{p}{\mu}}\frac{1}{q}\left[(q+1)\sin L + g\right] & \sqrt{\frac{p}{\mu}}\frac{f}{q}\left[h\sin L - k\cos L\right] \\ 0 & 0 & \sqrt{\frac{p}{\mu}}\frac{s^2\cos L}{2q} \\ 0 & 0 & \sqrt{\frac{p}{\mu}}\frac{s^2\sin L}{2q} \\ 0 & 0 & \sqrt{\frac{p}{\mu}}\frac{1}{q}\left[h\sin L - k\cos L\right] \\ 0 & 0 & 0 \end{bmatrix} \tag{14}$$

$$q = 1 + f\cos L + g\sin L \tag{15}$$

$$s^2 = 1 + h^2 + k^2 \tag{16}$$

Applying Pontryagin's Minimum Principle, the optimal thrust direction unit vector that minimizes the Hamiltonian (Eq. 3) may be found using Eq. 17.

$$\boldsymbol{u}^* = -\frac{\boldsymbol{B}^T\boldsymbol{\lambda}}{||\boldsymbol{B}^T\boldsymbol{\lambda}||} \tag{17}$$

The switch functions may be found using the same approach as in the polar coordinates formulation: collect on the terms including the throttle and reverse the sign of the resultant expression. Equation 18 describes the switch function for each mode. Note the costate for the spacecraft mass must be included separately because there is no contribution from that term in the $\boldsymbol{B}$ matrix.

$$S_i = \frac{T_i}{c_i}\left(\frac{c_i}{m}||\boldsymbol{B}^T\boldsymbol{\lambda}|| + \lambda_m - 1\right) \tag{18}$$

Finally, the throttles may be found at every instant using Eqs. 8-11 and Eq. 6 governs the costate dynamics.

C. Propellant-Constrained Minimum-Time Problem: MEEs—Penalty Function Approach

The cost functional, in Lagrange form, for the canonical minimum-time problem is given in Eq. 19. To solve the PCMT problem, the cost functional is augmented with a penalty function that enforces an inequality constraint on the propellant consumed by the high thrust mode. The augmented cost functional is shown in Eq. 20. The penalty function makes use of hyperbolic tangent smoothing (similar to the throttles in Eqs. 8-9). In that term, m_2 is the consumed propellant mass in mode 2, b is the allowable mass constraint, and ρ_c is a homotopy parameter. K is a multiplier that can be any value to aid convergence. Using a penalty function makes the propellant constraint a "soft constraint." That is, the second term approaches a value of 1 as the m_2 approaches b and ρ_c is decreased, but m_2 is not rigidly enforced to be less than or equal to b. Since the penalty function cost approaches 1 (prior to integration), it is of similar magnitude to the original minimum-time cost term and thus K may be set to 1. Using hyperbolic tangent smoothing greatly improves numerical convergence over a function that is strictly either 0 or 1 (or another large value).

$$J = \int_{t_0}^{t_f} 1dt = \int_{t_0}^{t_f} Ldt \tag{19}$$

$$J = \int_{t_0}^{t_f} 1 + \frac{1}{2}\left(\tanh\left(\frac{m_2 - b}{\rho_c}\right) + 1\right)Kdt = \int_{t_0}^{t_f} Ldt \tag{20}$$

The equations of motion may still be represented by Eq. 12, however the total spacecraft mass state used in the minimum-fuel formulation has been replaced by propellant consumed in each mode. These values are represented by m_1 and m_2 respectively. As a result, the final two terms of the $\boldsymbol{A}$ vector (Eq. 21) contain the differential equations for m_1 and m_2. The $\boldsymbol{B}$ matrix (Eq. 22) contains two rows of zeros to correspond to these additional differential equations. Equations 15-16 continue to define q and s^2, respectively, while Eq. 23 can be used to find the total remaining spacecraft mass. The initial spacecraft mass is represented by m_0.

$$\boldsymbol{A} = \begin{bmatrix} 0 & 0 & 0 & 0 & 0 & \sqrt{\mu p}\left(\frac{q}{p}\right)^2 & \frac{T_1}{c_1}\delta_1 & \frac{T_2}{c_2}\delta_2 \end{bmatrix}^T \tag{21}$$

$$\boldsymbol{B} = \begin{bmatrix} 0 & \frac{2p}{q}\sqrt{\frac{p}{\mu}} & 0 \\ \sqrt{\frac{p}{\mu}}\sin L & \sqrt{\frac{p}{\mu}}\frac{1}{q}\left[(q+1)\cos L + f\right] & -\sqrt{\frac{p}{\mu}}\frac{g}{q}\left[h\sin L - k\cos L\right] \\ -\sqrt{\frac{p}{\mu}}\cos L & \sqrt{\frac{p}{\mu}}\frac{1}{q}\left[(q+1)\sin L + g\right] & \sqrt{\frac{p}{\mu}}\frac{f}{q}\left[h\sin L - k\cos L\right] \\ 0 & 0 & \sqrt{\frac{p}{\mu}}\frac{s^2\cos L}{2q} \\ 0 & 0 & \sqrt{\frac{p}{\mu}}\frac{s^2\sin L}{2q} \\ 0 & 0 & \sqrt{\frac{p}{\mu}}\frac{1}{q}\left[h\sin L - k\cos L\right] \\ 0 & 0 & 0 \\ 0 & 0 & 0 \end{bmatrix} \tag{22}$$

$$m = m_0 - (m_1 + m_2) \tag{23}$$

While the optimal thrust direction unit vector remains as defined in Eq. 17, the switch functions are now given by Eq. 24.

$$S_i = \frac{T_i}{c_i}\left(\frac{c_i}{m}||\boldsymbol{B}^{\boldsymbol{T}}\boldsymbol{\lambda}|| - \lambda_{m_i}\right) \tag{24}$$

The approach to finding the optimal throttles (Eqs. 8-11) remains as described in the previous two sections with one exception: the penalty function term only appears in H_2 and not in H_1. Since that term exclusively pertains to the propellant mass consumed by mode 2, it is irrelevant to mode 1 and thus must only be included in H_2. The remainder of the procedure is the same as before.

D. Propellant-Constrained Minimum-Time Problem: MEEs—Interior-Point Constraint Approach

An alternative approach to solving the PCMT problem requires formulating the problem with an interior-point constraint. An interior-point constraint refers to a set of boundary conditions on the interior of a multi-point boundary value problem. At the interior-point, one or more costates, the Hamiltonian, or both may be discontinuous [23]. While the results shown in this paper were generated using the approach detailed in Section II.C, the following approach was found to produce nearly identical results.

The minimum-time cost functional in Mayer form is given in Eq. 25.

$$J = t_f \tag{25}$$

Assuming that 1) only one mode may be active at a time, 2) mode 1 corresponds to the lower-thrust, higher-specific impulse mode, and 3) $\frac{T_1}{c_1} < \frac{T_2}{c_2}$, the engine throttles are defined on the set shown in Eq. 26.

$$\{\delta_1, \delta_2 \in U \mid 0 \le \delta_1 \le 1,\ 0 \le \delta_2 \le 1,\ \delta_1 \cdot \delta_2 = 0\} \tag{26}$$

Equation 27 shows the mode 2 propellant mass constraint that ensures the propellant consumption remains less than or equal to the user-supplied value, b.

$$C(x,t) = m_2(t) - b \le 0 \tag{27}$$

The dynamics may again be described by Eq. 12. In this approach, the state variables were assumed to be the six MEEs, the total spacecraft mass, m, and the mass of the propellant consumed in mode 2, m_2. Thus, the $\boldsymbol{A}$ vector and $\boldsymbol{B}$ matrix for this problem are identical to those given in Eqs. 13-14 with the exception of an additional row in each corresponding to m_2. The final value in Eq. 13 is now $\frac{T_2}{c_2}\delta_2$ while the additional row in Eq. 14 is all zeroes.

The Hamiltonian, with the additional state constraint (see Ref. [23]), for this formulation is given in Eq. 28. In this expression, $\mu(t)$ is an additional Lagrange multiplier that is equal to zero when $C < 0$ (i.e., the constraint is active) and greater than or equal to zero when $C \ge 0$ (i.e., the constraint is active).

$$H = \boldsymbol{\lambda}^T \boldsymbol{f} + \mu(t)\dot{C}(x,t) \tag{28}$$

The necessary conditions of optimality require $\dot{C} = \delta_2 \frac{T_2}{c_2} = 0$ on the constraint boundary [23]. Accordingly, δ_2 must be zero when $m_2 = b$. Since $\dot{C}$ does not depend on the states, the term $\mu(t)\dot{C}$ is always zero and does not affect the Hamiltonian nor the costate dynamics.

Reaching the propellant constraint corresponds to the interior-point constraint. At that point, the change in the Hamiltonian is zero, per Eq. 29. λ_{m_2}, however, changes per Eq. 30. In both expressions, π is an additional Lagrange multiplier.

$$\Delta H = -\pi \frac{\partial C}{\partial t} = 0 \tag{29}$$

$$\Delta \lambda_{m_2} = \pi \frac{\partial C}{\partial m_2} = \pi \tag{30}$$

Since $\dot{\lambda}_{m_2} = -\frac{\partial H}{\partial m_2} = 0$ and $\lambda_{m_2}(t_f) = 0$ because the final state is free, there are two possible cases:

1) If the constraint, C, is never reached (i.e., the entire transfer can be completed in the given time without exceeding the mass requirement for mode 2), then $\lambda_{m_2}(t) = 0$ and mode 2 is always on.
2) If the constraint is reached, then $\lambda_{m_2}(t) = \pi$ while $C < 0$ and $\lambda_{m_2}(t) = 0$ when $C = 0$. This means $\lambda_{m_2}(t)$ is piecewise constant and the value of π must be determined.

After substituting Eq. 17 into Eq. 28, the switch functions for each mode may be found as before. These are shown in Eqs. 31-32.

$$S_1 = ||B^T\lambda|| \frac{T_1}{m} + \lambda_m \frac{T_1}{c_1} \tag{31}$$

$$S_2 = ||B^T\lambda|| \frac{T_2}{m} + \lambda_m \frac{T_2}{c_2} - \lambda_{m_2} \frac{T_2}{c_2} \tag{32}$$

Since $T_2 > T_1$ and $\frac{T_2}{c_2} > \frac{T_1}{c_1}$ by hypothesis, if $\lambda_{m_2}(t) = 0$ (case 1 above), S_2 is always greater than S_1. This implies that mode 2 is always on. If, instead, $\lambda_{m_2}(t) \neq 0$ (case 2 above), then S_2 may be larger or smaller than S_1, depending on the values of λ_m and λ_{m_2}. Accordingly, the throttles may be found using Eqs. 33-34.

$$\delta_1^* = \begin{cases} 0 & \text{for } S_2 > S_1 \text{ and } m_2 < b \\ 1 & \text{for } S_1 > S_2 \text{ or } m_2 = b \end{cases} \tag{33}$$

$$\delta_2^* = 1 - \delta_1^* \tag{34}$$

Equation 33 (and thus Eq. 34) are inherently non-smooth. Thus, two approaches for implementation have been considered:

1) Use event detection within the ordinary differential equation (ODE) solver (see Section II.E) to detect when $S_1 - S_2 = 0$ and $m_2 = b$. Then, apply Eqs. 33-34. In this approach, the throttle values are always strictly zero or one.
2) Apply hyperbolic tangent smoothing to the throttles using a composite switching function.

The former relies on the capabilities of the ODE solver being used and may not be simple to implement. The latter approach (which was initially investigated) requires the modification of Eq. 32 to include the mass constraint. The new switch function for mode 2 is shown in Eq. 35. Note ρ_c is a homotopy parameter within the switch function.

$$S_2 = \frac{1}{2}\left(1 - \tanh\left(\frac{m_2 - b}{\rho_c}\right)\right)\left(||B^T\lambda|| \frac{T_2}{m} + \lambda_m \frac{T_2}{c_2} - \lambda_{m_2} \frac{T_2}{c_2}\right) \tag{35}$$

Using Eq. 35, the optimal mode 1 throttle may be found as shown in Eq. 36. The mode 2 throttle is still defined by Eq. 34.

$$\delta_1^* = \frac{1}{2}\left(1 + \tanh\left(\frac{S_1 - S_2}{\rho}\right)\right) \tag{36}$$

As before, the costate dynamics may be found using Eq. 6.

E. Numerical Approach

Each problem was implemented in MATLAB as a two-point boundary value problem (TPBVP). For the minimum-fuel problems, the time-of-flight was fixed. The time-of-flight is an unknown in the PCMT problem and thus the additional transverality condition $H(t_f) = 0$ must be met as a part of the TPBVP. Canonical units were used to improve convergence behavior.

MATLAB's Symbolic Toolbox was used to generate a script containing the system dynamics. Symbolic differentiation was used to create the costate differential equations within said script. To solve the problem, the Levenberg-Marquardt [44, 45] algorithm within MATLAB's intrinsic `fsolve.m` function was used to find the initial costates that yield a trajectory that satisfies the final boundary conditions. A function tolerance of $1 * 10^{-12}$ and a step tolerance of $1 * 10^{-14}$ were used within `fsolve.m`. At every time step, the equations of motion were propagated using MATLAB's intrinsic `ode89.m` (relative tolerance of $1 * 10^{-12}$ and an absolute tolerance of $1 * 10^{-14}$) function, which uses a Runge-Kutta 9(8) pair method [46]. Note that `ode45.m` (based on a Runge-Kutta (4,5) method [47, 48]) can also be used for propagation. MATLAB's `fsolve.m` updates the initial guess until the convergence criteria are met. Note that a MATLAB MEX file (a MATLAB created and callable compiled function that runs in either C or C++) was created for the function being solved by `fsolve.m` to greatly increase the computational speed of the solver.

Only a single homotopy parameter, ρ, needed to be swept to its final, user-supplied value for the minimum-fuel problems. Upon reaching this point, the time-of-flight could then be changed manually or in a loop and the homotopy process could be repeated to find the final desired trajectory. For the PCMT problems, ρ and ρ_c had to be swept to their final values. The most consistent convergence was found by first reducing the value of ρ prior to beginning the continuation process on ρ_c. After completing all of the necessary continuation, the output from `fsolve.m` was propagated and the results were plotted.

All three problems solved in this study, like many indirect optimal control problems, were found to be very sensitive to the initial guess for the costates (and time-of-flight for the PCMT problem). To develop a suitable initial guess for the minimum-fuel transfers, a single mode minimum-time problem was first solved using the low-thrust mode. This provides an upper bound on the multimode trajectory duration. A minimum-fuel problem with a time-of-flight shorter than the low-thrust minimum-time transfer was then solved using only the high-thrust mode. The resultant initial guess was then used to warm-start the multimode minimum-fuel transfers. For the PCMT transfers, the initial guess was generated from a minimum-fuel transfer using the same modes and additional manual adjustment to yield convergence. Specific paths to convergence are described in Section III alongside the sample trajectories.

III. Results

This section describes sample results for each of the problems presented in Section II. The emphasis here is on development and exploration of the techniques rather than the design of a specific trajectory. As such, all trajectories presented are feasible and (at least) locally optimal, but do not necessarily represent a specific mission, spacecraft, or near-term propulsion technology.

A. Minimum-Fuel Problem: Polar Coordinates

A two-dimensional, minimum-fuel transfer from Earth's orbit to Mars's orbit was found using the approach outlined in Section II.A. For this transfer, the thruster was assumed to have two modes: a 0.235 N, 4,155 s mode and a 0.5 N, 1,000 s mode. The former is representative of the maximum power mode of NASA's NEXT-C [49] thruster while the second mode was chosen to aid convergence. These modes require a minimum of 4.8 kW and 2.5 kW of power to operate (assuming perfect efficiency). As such, this combination of modes does not represent a near-term multimode propulsion system and were instead chosen to demonstrate the technique presented here. The modes used for this trajectory are summarized in Table 1.

To find a solution, a minimum-time problem was first solved using only mode 1. A 256.78 day transfer was found. This time-of-flight informs the feasible length of a multimode transfer (i.e., the time-of-flight should be less than the low-thrust only minimum-time solution). A 240 day minimum-fuel problem was then solved using only mode 2. The

Table 1 Thruster performance summary: Earth-Mars transfer

	Thrust (N)	I_{sp} (s)
Mode 1	0.235	4,155
Mode 2	0.5	1,000

resulting initial guess was used to warm-start the multimode solution. Due to initial convergence challenges, mode 1 was slowly turned on (i.e., its thrust value was swept to its final value) prior to performing any homotopy. This technique was sufficient to find an initial multimode solution and permit the homotopy process to proceed.

Figure 1 depicts a 240 day transfer from Earth to Mars for a 500 kg spacecraft in the Sun-centered inertial frame. The Sun is located at the origin. The radial distances are given in astronomical units. The trajectory begins at Earth, represented with a green marker, and concludes at Mars, represented with an orange marker. The blue portion of the trajectory corresponds to the lower-thrust mode while the red corresponds to the higher-thrust mode. The arrows indicate the thrust direction vector and are normalized to the throttle setting (which takes on values between 0 and 1). The trajectory has terminal high-thrust burns with lower-thrust burns in the middle of the trajectory. A single coast arc is represented by the portion of the trajectory in black and without arrows.

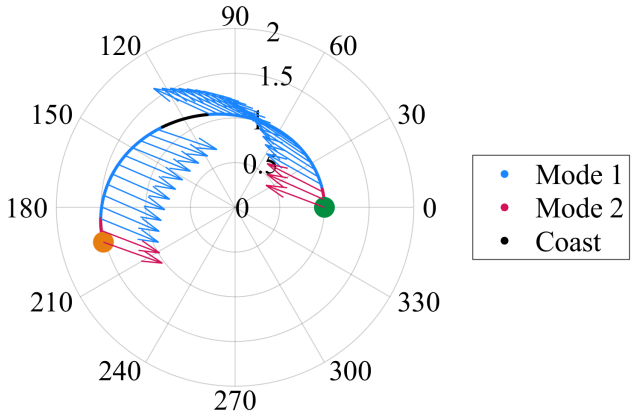

Fig. 1 Earth-Mars transfer trajectory

The switch functions and the corresponding throttle settings are shown in Fig. 2. Using the convention outlined in Section II.A, a mode may be active when its switch function is greater than zero. Thus, the coast arc occurs when both switch functions are less than zero. The coast period begins approximately 101 days into the transfer and lasts 29.2 days.

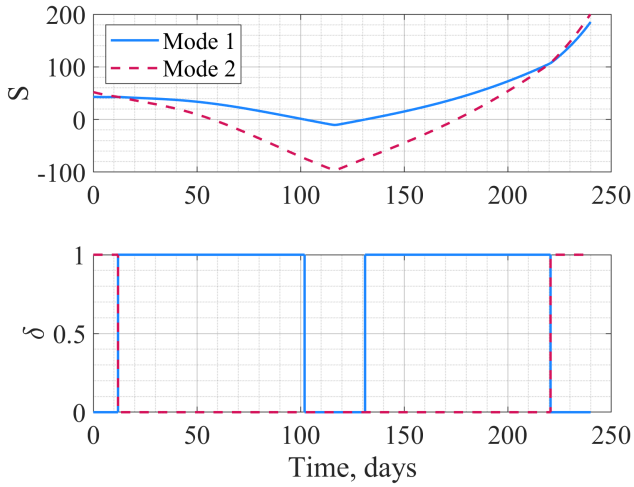

Fig. 2 Switch function (top) and throttle magnitude (bottom) for the Earth-Mars transfer

The time histories of the states and their corresponding costates are shown in Fig. 3. The initial boundary conditions of this problem were that the spacecraft begins at a radial distance of 1 AU with Earth's velocity. Since circular orbits are assumed by the polar coordinate representation, the spacecraft begins with only transverse velocity. An initial angular position of zero was assumed. At the conclusion of the transfer, the spacecraft is required to match the position and velocity of Mars's orbit. Because this trajectory was not designed to satisfy a particular planetary alignment, an arbitrary final angular position of 3.4 rad (≈194.8°) was selected. Since the final spacecraft mass is unknown, the mass costate must be equal to zero at the final time to satisfy the transversality condition. This figure reveals that the boundary conditions are satisfied by this trajectory.

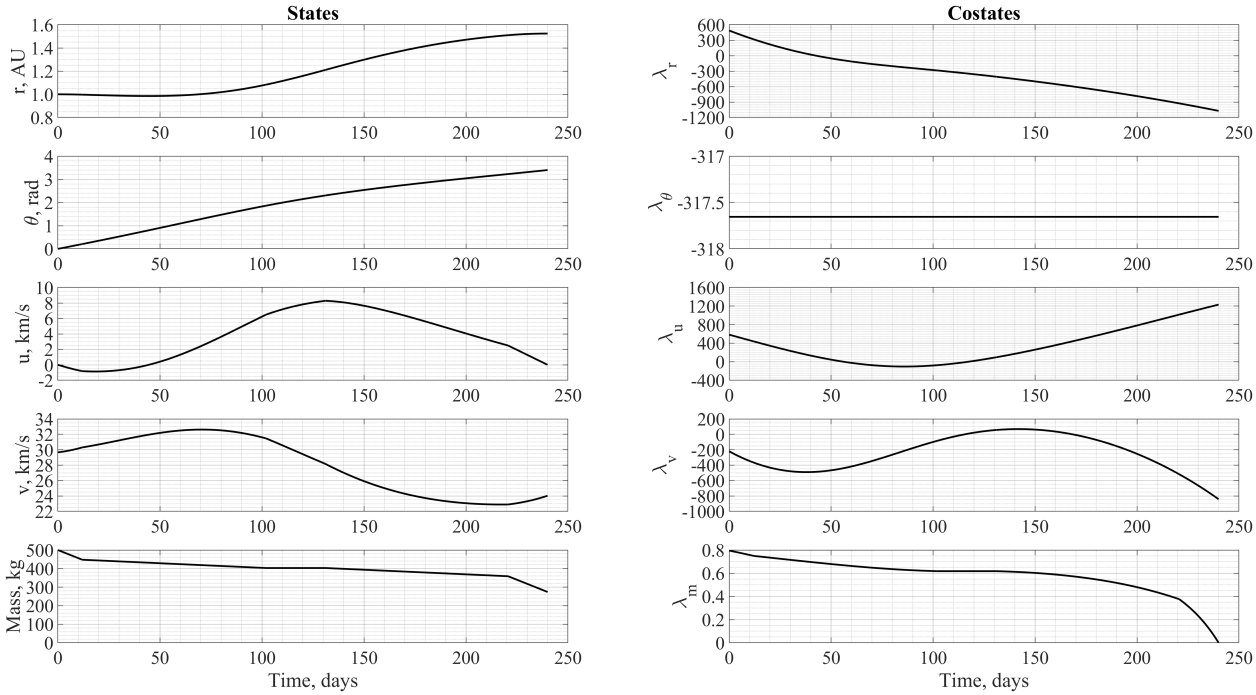

Fig. 3 Time histories of the states and costates for the Earth-Mars transfer

Since this transfer is a minimum-fuel trajectory, the cost is represented by the propellant consumed. Figure 4 depicts the propellant consumption as a function of time and operating mode (n.b., this figure depicts mass consumed while the bottom right subplot in Fig. 3 shows total remaining spacecraft mass). The modes are, again, represented by color

on this plot, though the slope of each line segment may also be used to identify the mode of operation because it corresponds to the mass flow rates. Thus, the steeper line segments correspond to the 0.5 N mode while the less steep segments correspond to the 0.235 N mode. The transfer consumes a total of 226.14 kg propellant, with 88.97 kg used by mode 1 and 137.17 kg used by mode 2. Mode 1 operates for a total of 149.08 days between the two burns while mode 2 operates for 226.14 days. Both modes operate twice. The mode usage in this transfer is summarized in Table 2.

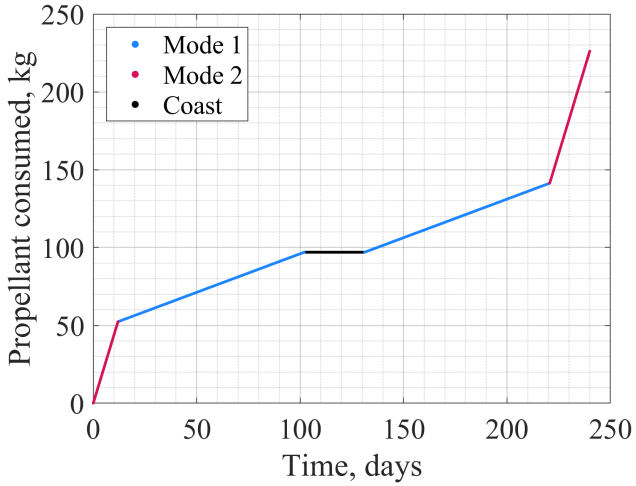

Fig. 4 Accumulated propellant consumption for the Earth-Mars transfer

Table 2 Mode usage summary for the Earth-Mars transfer

	Propellant Consumed (kg)	Total Burn Time (days)	Number of Startups
Mode 1	88.97	149.08	2
Mode 2	226.14	71.72	2

The components of the thrust unit vector are shown in Fig. 5. The top subplot, u_1, is the radial component while the bottom subplot, u_2, is the tangential component. While the profiles are generally fairly smooth, there is a cusp approximately 115 days into the trajectory. This, however, occurs during the coast period and thus could be mitigated via a smooth pointing profile commanded by the operations team.

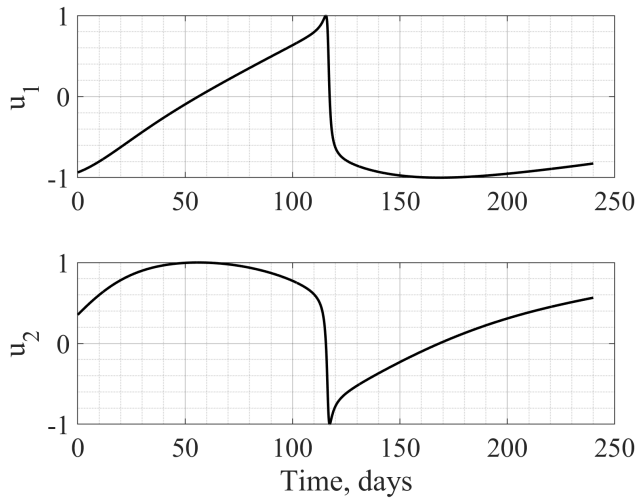

Fig. 5 Control direction unit vector components for the Earth-Mars transfer

Figure 6 depicts the value of the total Hamiltonian, H, the Hamiltonians corresponding to each mode, H_1 and H_2, along with the throttle values, δ_1 and δ_2. While Fig. 3 reveals that the trajectory satisfies the TPBVP and the transverality condition on the spacecraft mass costate, Fig. 6 allows assessment of the optimality of the transfer. For the transfer to be optimal, the mode selected at every instant must minimize the total Hamiltonian. This figure shows this condition is met (i.e., $\delta_1 = 1$ when $H_1 \leq H_2$ and $\delta_2 = 1$ when $H_2 < H_1$). Thus, this transfer satisfies the necessary conditions for optimality.

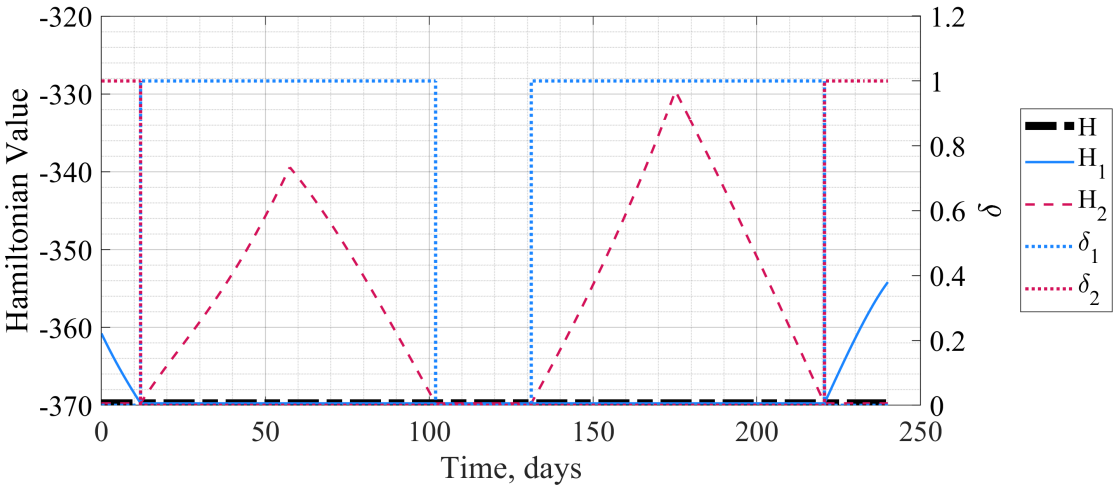

Fig. 6 Hamiltonian value with throttle magnitude for the Earth-Mars transfer

Multimode minimum-fuel trajectories with other times-of-flight (and the same boundary conditions) may readily be found using the above converged solution to warm-start other solutions. As a result, a Pareto front can be created that compares multimode solutions to trajectories that only use one of the two modes. In Fig. 7, multimode solutions are represented by black circles while trajectories using mode 1 only are shown with blue stars. Red diamonds mark mode 2 only solutions. The vertical dashed line marks the minimum-time solution for a spacecraft with only mode 1 available. Left of that line (at 256.78 days), the higher thrust mode is required to reduce the time-of-flight. Having the lower-thrust mode available allows the multimode system to save between approximately 20 and 75 kg of propellant in comparison to the mode 2 only results. To the right of the dashed line, only mode 1 is required to complete the transfer. Several of the mode 1 only solutions overlap with the multimode solutions. The 280 and 285-day mode 1 transfers, however, require the spacecraft to go beyond the final orbit and return to meet the final position requirement. This is

suboptimal in comparison to the multimode system that can use the higher thrust mode to alleviate this issue. While the 240 day transfer detailed here does not necessarily represent a specific mission, nor does it use a near-term multimode propulsion system, the analysis presented in Fig. 7 is representative of the trade studies that can be conducted using the technique developed in this work.

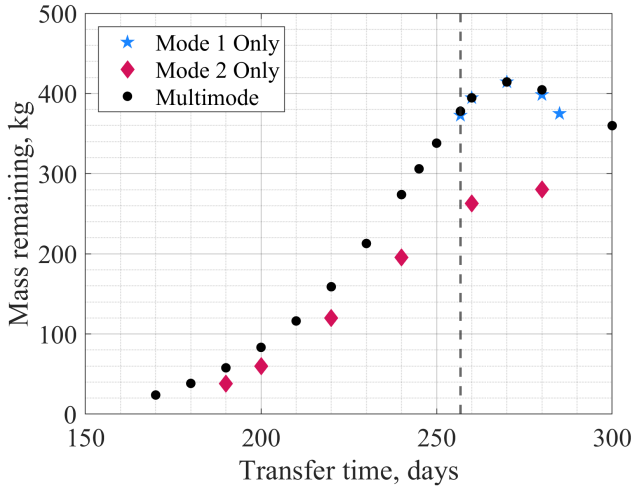

Fig. 7 Earth-Mars transfer Pareto front

B. Minimum-Fuel Problem: Mean Equinoctial Elements

A 4 day, minimum-fuel multimode transfer from GTO to GEO was found using the approach described in Section II.B. For this problem, a 0.5 N, 3,100 s mode was assumed for mode 1 and a 1 N, 250 s mode was chosen for mode 2. These settings are summarized in Table 3. This combination of modes, while infeasible with present multimode systems, is representative of a future, high-power chemical-electric multimode system (n.b., mode 1 would require, at minimum, 7.6 kW for operation). The spacecraft was assumed to have an initial mass of 100 kg.

Table 3 Thruster performance summary: GTO-GEO transfer

	Thrust (N)	I_{sp} (s)
Mode 1	0.5	3,100
Mode 2	1	250

The GTO to GEO transfer is shown in Fig. 8 in the Earth-centered inertial reference frame. The top left subplot provides a three-dimensional view while the remaining subplots show various projections of the trajectory. As in the previous section, blue corresponds to mode 1 and red to mode 2. This trajectory does not have a coast arc. To find this trajectory, the solution was warm-started with an initial guess for a mode 2 only minimum-fuel trajectory (which was reasonably easy to find with a random initial guess). Like in the previous section, mode 1 was slowly turned on until an initial solution was found and the homotopy procedure could be followed.

The initial orbit (GTO) was assumed to have a semi-major axis of 24,505 km, an eccentricity of 0.725, and 7° of inclination. The remaining classical orbital elements were assumed to be zero. The final orbit (GEO) was assumed to have a semi-major axis of 42,165 km, zero eccentricity, and zero inclination. A final true longitude of 53.4 rad was assumed (approximately 8.5 revolutions about the Earth). The final right ascension of the ascending node and argument of periapsis are undefined due to GEO being circular and non-inclined and thus do not impact the final MEEs.

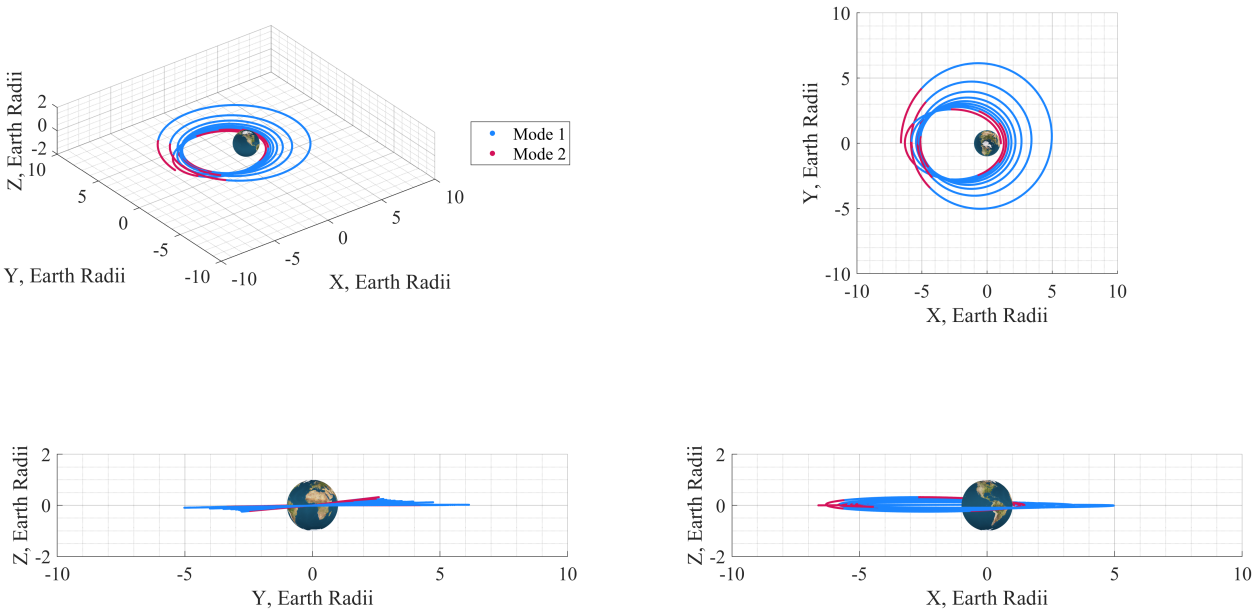

Fig. 8 GTO-GEO minimum-fuel trajectory with projections

The time histories of the semi-major axis, a, eccentricity, e, and inclination, i, are shown in Fig. 9. This figure reveals the eccentricity and inclination are significantly reduced prior to any large changes in the orbit size.

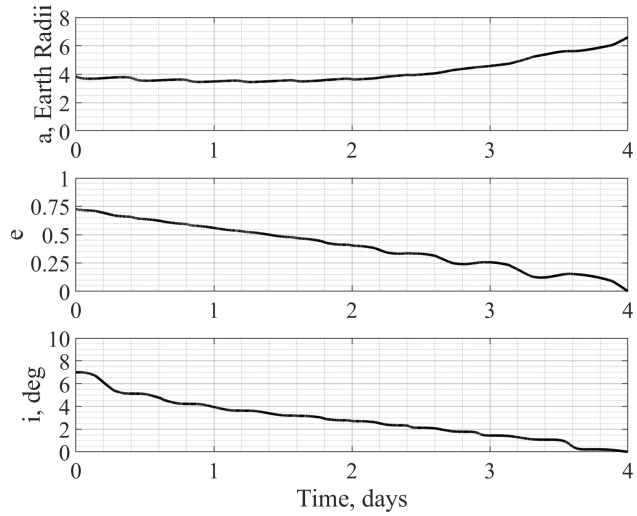

Fig. 9 Time history of the Keplerian States for the GTO-GEO transfer

The values of the switch functions and the throttle settings are shown in Fig. 10. This figure reveals ten mode 2 and nine mode 1 burns were required to complete the minimum-fuel transfer. No coast arc is present in this solution.

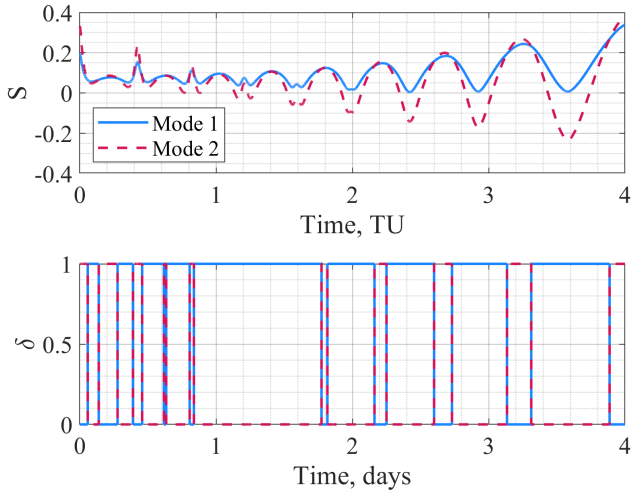

Fig. 10 Switch function (top) and throttle magnitude (bottom) for the GTO-GEO transfer

Figure 11 depicts the time histories of the states and the costates used to solve this problem. This figure, along with Fig. 9, confirms the solution meets the boundary conditions and spacecraft mass costate transversality condition. Generally, the profiles for each state and costate are smooth, if occasionally oscillatory.

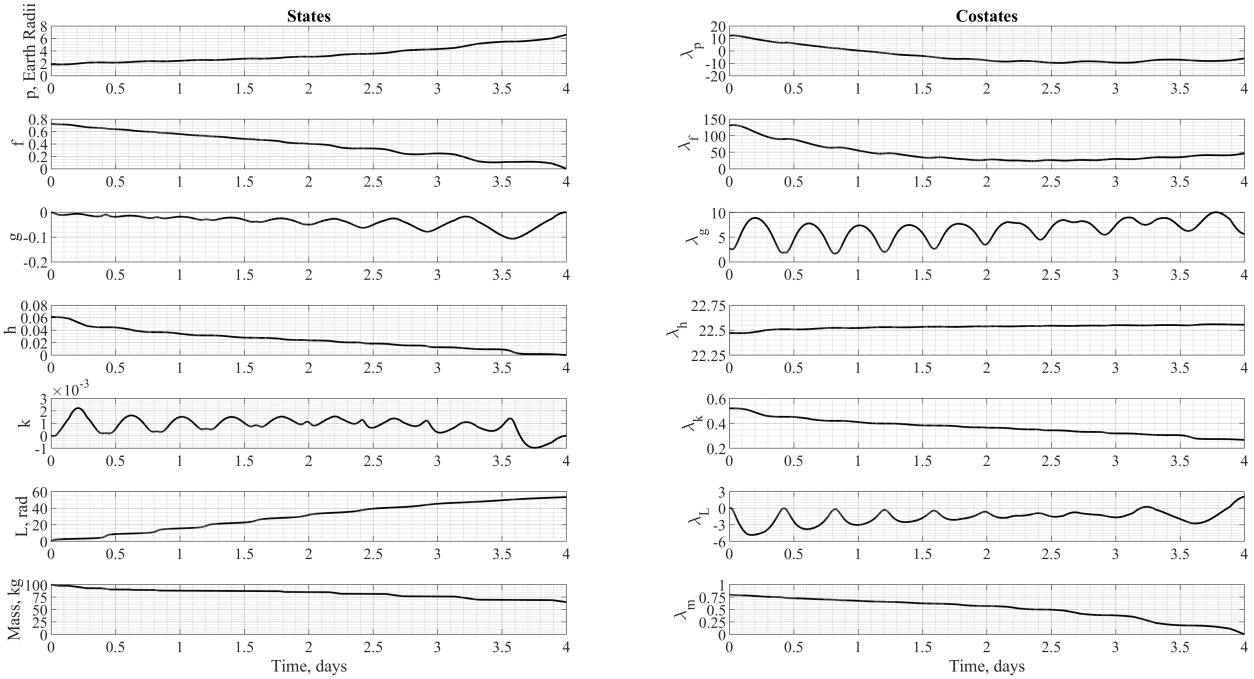

Fig. 11 Time histories of the states and costates for the GTO-GEO transfer

The accumulated propellant consumption is shown in Fig. 12. Again, each line segment is colored to correspond to the relevant mode and the slopes can also be used to identify the mode of operation. This trajectory consumes a total of 34.92 kg of propellant: 4.46 kg are consumed by mode 1 and 30.46 kg are used in mode 2. The final spacecraft mass is 65.08 kg.

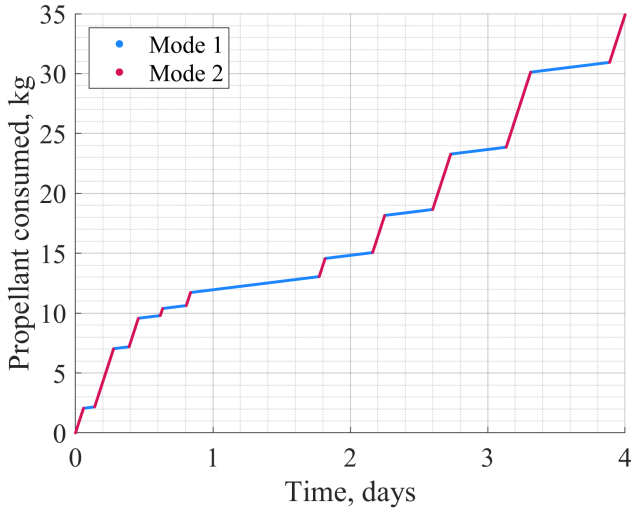

Fig. 12 Accumulated propellant consumption for the GTO-GEO transfer

The components of the thrust direction unit vector, in the spacecraft's radial-transverse-normal (RTN) reference frame, are shown in Fig. 13. While there are several rapid changes in the thrust direction unit vector, none of the reversals are instantaneous. As an example, the fastest direction change in the radial direction occurs over approximately 45 minutes. Further system-specific analysis would be required to determine if that rate is acceptable.

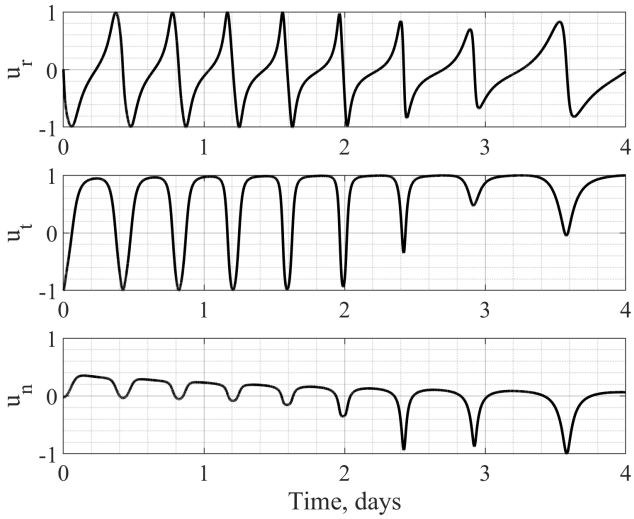

Fig. 13 Control direction unit vector components for the GTO-GEO transfer

Table 4 compares the multimode trajectory detailed above to a mode 1 minimum-time trajectory and to a mode 2 minimum-fuel trajectory (4 day time-of-flight) with the same boundary conditions. The mode 1 minimum-time transfer takes 5.20 days and consumes 7.39 kg of propellant. The mode 2 minimum-fuel transfer consumes 52.58 kg of propellant. The multimode solution, as would be anticipated, lies between these results. Having a higher thrust mode available allows a reduction in the time-of-flight in comparison to the low-thrust only solution while also saving 17.66 kg of propellant in comparison to the mode 2 results. It is important to note the multimode solution does not have a coast arc. This may be challenging due to thruster lifetime limitations or operational considerations (i.e., communications, ranging, etc.). The mode 2 solution, however, operates for 36.75% of the transfer time, providing opportunities for other spacecraft activities. To alleviate this issue, the technique described in Ref. [37] could be used to force a coast arc to occur. The number of startups for each mode are also listed in Table 4 because the total number may have thruster lifetime implications. While the multimode spacecraft and its propulsion system are notional, the results demonstrate

the typical benefits of multimode propulsion in comparison to traditional architectures.

Table 4 Propellant consumption comparison: GTO-GEO transfer

	Total Transfer Time (days)	Propellant Consumed (kg)	Burn Time (days)	Number of Startups
Mode 1 only (min. time)	5.20	7.39	5.20	1
Mode 2 only (min. fuel)	4	52.58	1.47	10
Multimode: Mode 1	4	4.46	3.14	10
Multimode: Mode 2		30.46	0.86	9

C. Propellant-Constrained Minimum-Time Problem: Mean Equinoctial Elements

The same modes given in Table 3 were used to find a propellant-constrained minimum-time transfer in medium Earth orbit (MEO) using the method described in Section II.C. The results generated using the interior-point constraint approach (Section II.D) were found to be essentially identical and are omitted here for brevity. A 100 kg spacecraft was assumed to begin in an orbit with a semi-major axis of 24,505 km, an eccentricity of 0.1, and an inclination of 1°. The remaining orbital parameters were assumed to be zero. The final orbit was assumed to be circular, equatorial, and have a semi-major axis of 28,000 km. The transfer was completed in three revolutions.

Figure 14 shows the PCMT transfer, in the Earth-centered inertial reference frame, assuming a mode 2 mass constraint of 35 kg. This solution was warm-started using a mode 2 only solution that consumed 41.13 kg of propellant. For the multimode solution, homotopy was performed on the throttles prior to beginning homotopy on the penalty function term.

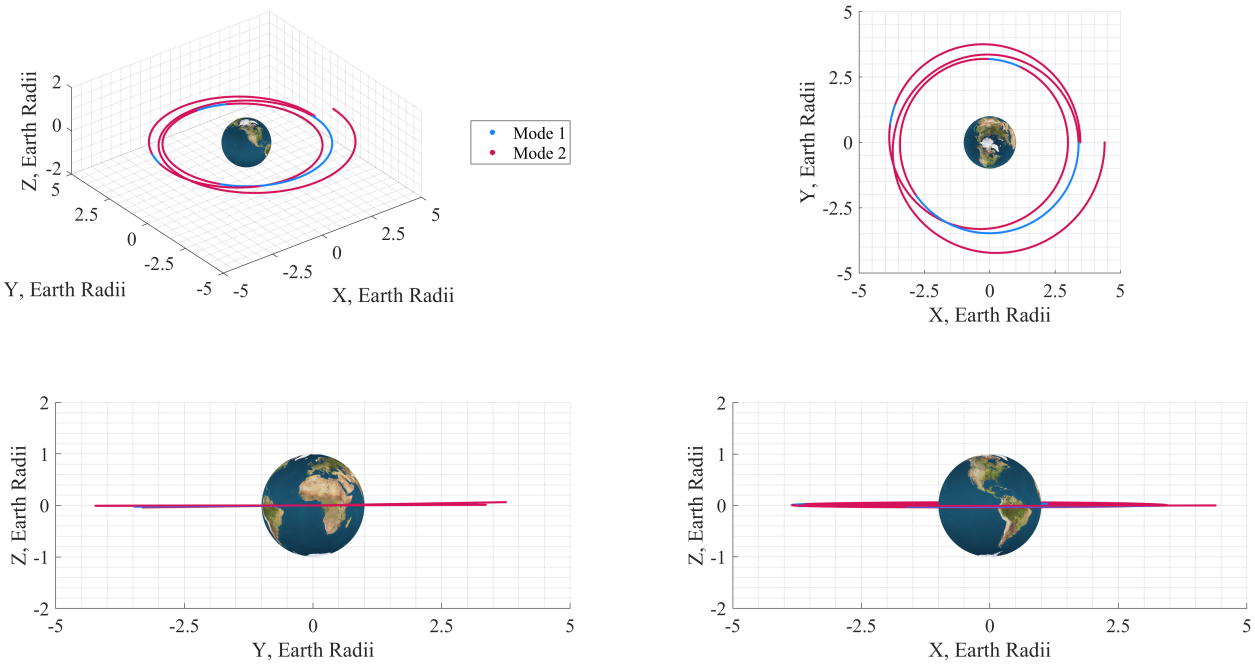

Fig. 14 PCMT trajectory with projections

The switch functions and throttles are shown in Fig. 15. This trajectory requires four high-thrust burns, including both terminal burns, and three low-thrust burns to meet the boundary conditions and mass constraint. The entire transfer occurs over 1.18 days.

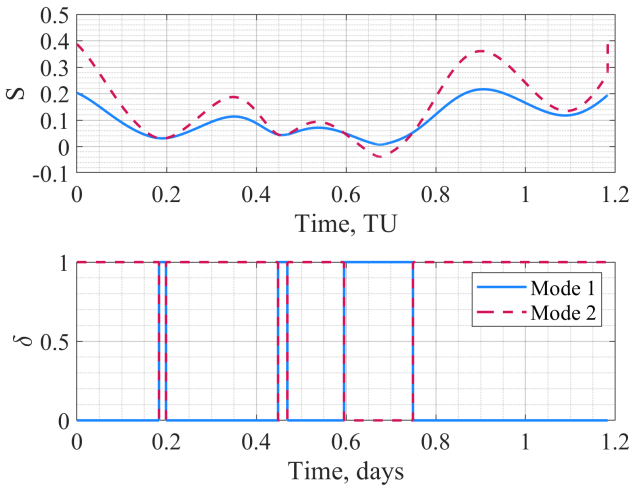

Fig. 15 Switch function (top) and throttle magnitude (bottom) for the PCMT transfer

The orbital states and costates for this trajectory are shown in Fig. 16. The states and costates corresponding to the propellant consumed in each mode are shown in Fig. 17. Figure 16 shows the orbital parameters vary smoothly throughout the trajectory. Figure 17 is, however, more notable. Since the value of the propellant consumed in each mode is free at the final time, their associated costates must be equal to zero. While the mode 1 propellant mass costate is smooth and continuous, the mode 2 propellant mass costate, shown in the bottom right of Fig. 17, exhibits a sharp discontinuity at the end of the trajectory. This occurs as m_2 approaches the 35 kg constraint (denoted by the red dashed line). This behavior suggests this trajectory may have an implicit interior-point constraint (see section II.D).

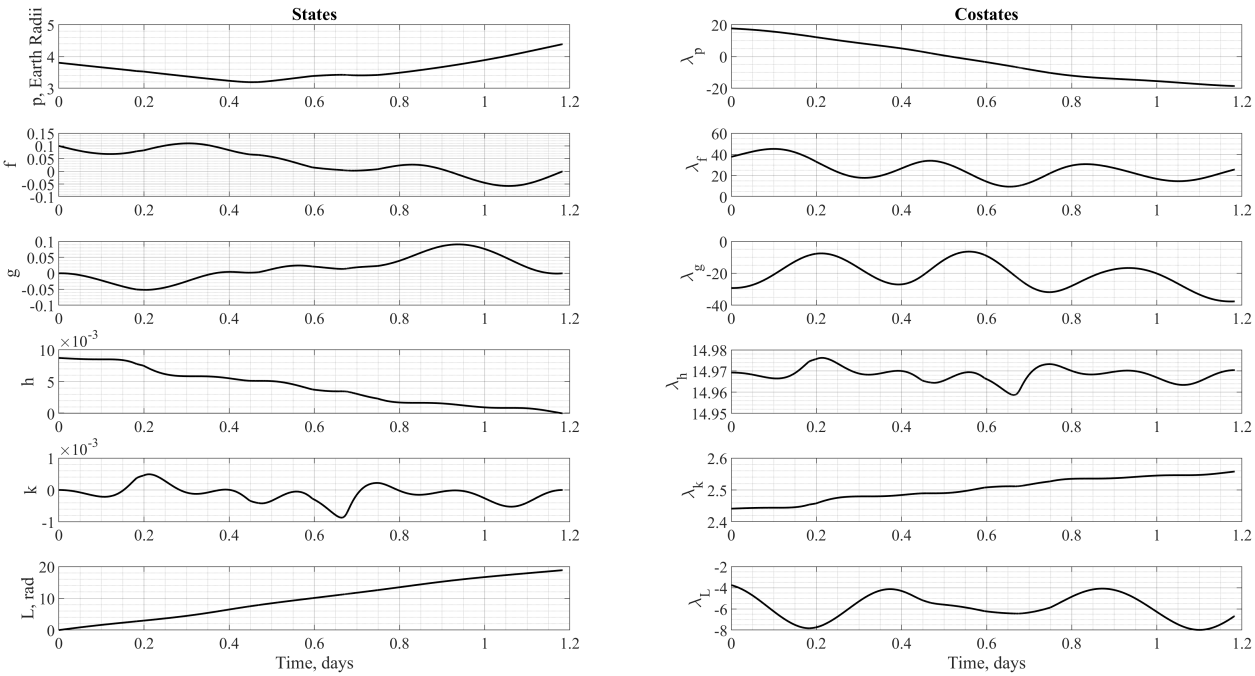

Fig. 16 Time histories of the orbital states and costates for the PCMT transfer

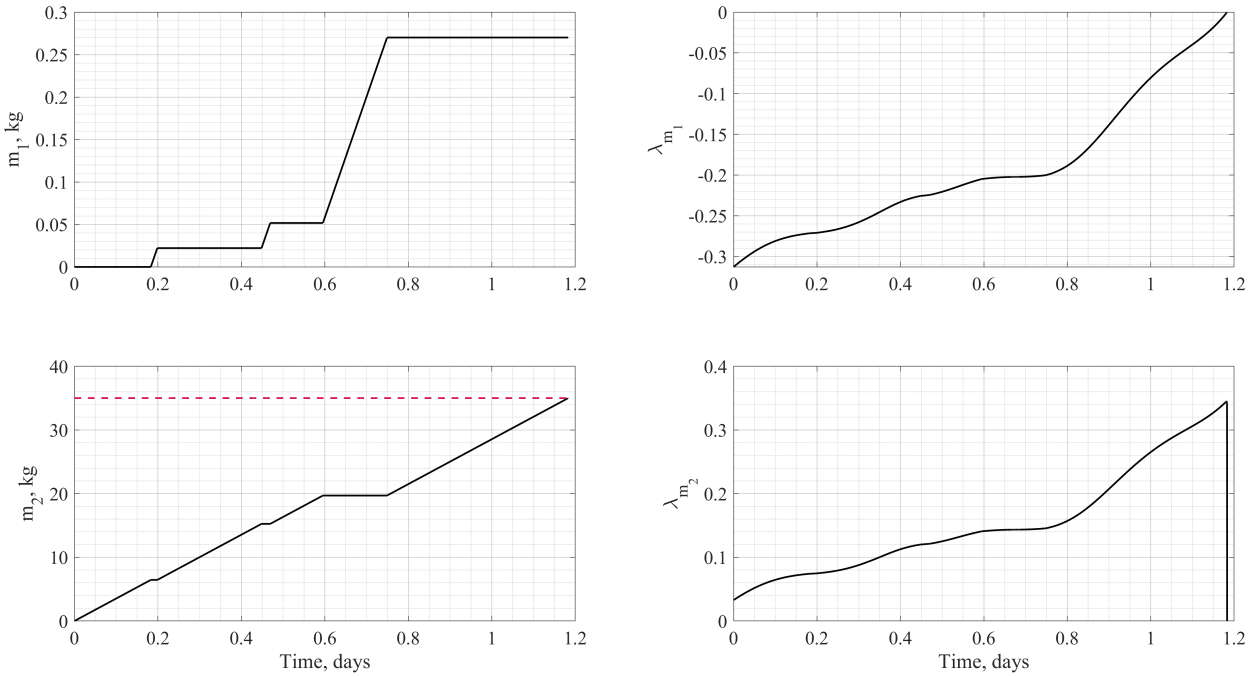

Fig. 17 Time histories of the propellant consumption and associated costates for the PCMT transfer

Figure 18 displays the Hamiltonian as a function of time. Because this is a minimum-time trajectory, the transfer time is unknown. Accordingly, the Hamiltonian must be equal to zero at the final time to meet the associated transversality condition. Here, the value is on the order of 10^{-9}. This is sufficiently close to zero given the tolerances used.

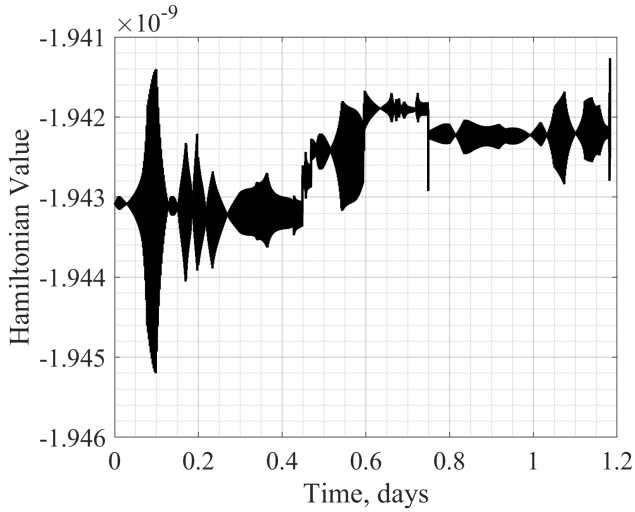

Fig. 18 Time history of the Hamiltonian for the PCMT transfer

The components of the thrust direction unit vector, again in the RTN frame, are shown in Fig. 19 as a function of time. Each of the components varies smoothly and continuously throughout the trajectory.

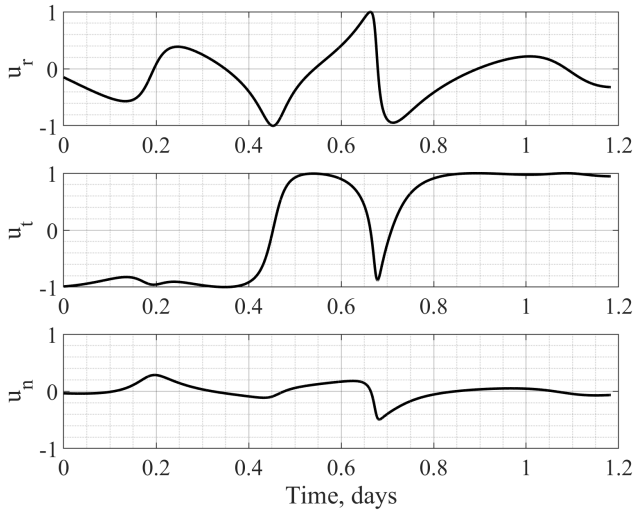

Fig. 19 Control direction unit vector components for the PCMT transfer

Table 5 compares minimum-time transfers using mode 1 only, mode 2 only, and the PCMT multimode solution presented above. The low-thrust only solution requires 1.93 kg of propellant and is completed in 1.36 days. The high-thrust solution has a 15% shorter time-of-flight than the low-thrust solution, but requires nearly 40 kg more propellant. The multimode solution presents a compromise: a 5.87 kg reduction in total propellant in comparison to the high-thrust trajectory with a time-of-flight 13% shorter than the low-thrust trajectory. Note the mode 2 propellant usage is 34.99 kg rather than 35 kg exactly because the penalty function enforces the constraint asymptotically rather than exactly. These values, of course, are problem dependent. Indeed, the mode 1 only solution may be the most intriguing in this scenario due to the significantly reduced propellant consumption and only a moderately longer time-of-flight than the other solutions. Other problems may find the multimode solution to be the most valuable.

Table 5 Propellant consumption comparison: MEO minimum-time transfer

	Total Transfer Time (days)	Propellant Consumed (kg)	Burn Time (days)	Number of Startups
Mode 1 only	1.36	1.93	1.36	1
Mode 2 only	1.16	41.13	1.16	1
Multimode: Mode 1	1.18	0.27	0.19	3
Multimode: Mode 2		34.99	0.99	4

IV. Conclusion

In this study, new indirect optimal control techniques were developed to solve multimode (or hybrid) minimum-fuel and PCMT transfers with automatic selection of the burn sequence. This is a significant advance over the current state-of-the-art for multimode mission design and enables future trajectory design efforts and trade studies. A key assumption of this approach is that only one mode may be active at a time. This is reasonable for most multimode and hybrid systems.

Multimode minimum-fuel trajectories were developed for an interplanetary transfer in polar coordinates and a GTO-GEO transfer in MEEs. The results showed the presented approach generates feasible trajectories that satisfy the necessary conditions of optimality. The multimode solutions were also found to provide the typical advantages of multimode propulsion: reduced transfer time in comparison to a low-thrust only trajectory and reduced propellant consumption in comparison to a high-thrust only trajectory.

Finally, applying penalty methods and hyperbolic tangent smoothing was found to be an effective technique for solving PCMT problems. The results showed the technique can be used to enforce significant reductions in propellant

mass over high-thrust only solutions. Although a simplistic transfer was described here, this technique is broadly applicable and may be extended to enforce additional constraints. This represents a significant contribution to the field that may have immediate impact on the design of future hybrid and multimode trajectories.

Funding Sources

This work was partially supported by the NASA SmallSat Technology Partnerships program, grant number 80NSSC20M0089.

Acknowledgments

The first author acknowledges Ruthvik Bommena for his insight and many fruitful conversations about the optimal control formulation.

References

[1] Rovey, J. L., Lyne, C. T., Mundahl, A. J., Rasmont, N., Glascock, M. S., Wainwright, M. J., and Berg, S. P., "Review of multimode space propulsion," *Progress in Aerospace Sciences*, Vol. 118, 2020. https://doi.org/10.1016/j.paerosci.2020.100627.

[2] Walker, M. J. H., Ireland, B., and Owens, J., "A set modified equinoctial orbit elements," *Celestial mechanics*, Vol. 36, No. 4, 1985, pp. 409–419. https://doi.org/10.1007/BF01227493.

[3] Gilland, J. H., "Synergistic Use of High and Low Thrust Propulsion Systems for Piloted Missions to Mars," *NASA Contractor Report 189138*, 1992.

[4] Mingotti, G., Topputo, F., and Massari, M., "Hybrid propulsion transfers for Mars science missions," *Proceedings of the 23rd AAS/AIAA Space Flight Mechanics Meeting*, Advances in the Astronautical Sciences, Vol. 148, Univelt, Inc., Kauai, HI, 2013, pp. 2859–2874.

[5] Percy, T., McGuire, M., and Polsgrove, T., "Combining Solar Electric Propulsion and chemical propulsion for crewed missions to Mars," *2015 IEEE Aerospace Conference*, 2015, pp. 1–10. https://doi.org/10.1109/AERO.2015.7119289.

[6] Chai, P., Merrill, R. G., and Qu, M., "Mars Hybrid Propulsion System Trajectory Analysis, Part I: Crew Missions," *AIAA SPACE 2015 Conference and Exposition*, 2015, pp. 1–15. https://doi.org/10.2514/6.2015-4443.

[7] Chai, P., Merrill, R. G., and Qu, M., "Mars Hybrid Propulsion System Trajectory Analysis, Part II: Cargo Missions," *AIAA SPACE 2015 Conference and Exposition*, 2015, pp. 1–12. https://doi.org/10.2514/6.2015-4444.

[8] Mani, K. V., Cervone, A., and Topputo, F., "Combined Chemical–Electric Propulsion for a Stand-Alone Mars CubeSat," *Journal of Spacecraft and Rockets*, Vol. 56, No. 6, 2019, pp. 1816–1830. https://doi.org/10.2514/1.A34519.

[9] Topputo, F., and Massari, M., "Modeling and Optimization of Hybrid Transfers to Near Earth Objects," *Space Engineering*, Vol. 114, edited by G. Fasano and J. D. Pintér, Springer International Publishing, Cham, 2016, pp. 425–442. https://doi.org/10.1007/978-3-319-41508-6_16.

[10] Oleson, S. R., Myers, R. M., Kluever, C. A., Riehl, J. P., and Curran, F. M., "Advanced Propulsion for Geostationary Orbit Insertion and North-South Station Keeping," *Journal of Spacecraft and Rockets*, Vol. 34, No. 1, 1997, pp. 22–28. https://doi.org/10.2514/2.3187.

[11] Mailhe, L. M., and Heister, S. D., "Design of a Hybrid Chemical/Electric Propulsion Orbital Transfer Vehicle," *Journal of Spacecraft and Rockets*, Vol. 39, No. 1, 2002, pp. 131–139. https://doi.org/10.2514/2.3791.

[12] Oh, D. Y., Randolph, T., Kimbrel, S., and Martinez-Sanchez, M., "End-to-End Optimization of Chemical-Electric Orbit-Raising Missions," *Journal of Spacecraft and Rockets*, Vol. 41, No. 5, 2004, pp. 831–839. https://doi.org/10.2514/1.13096.

[13] Kluever, C. A., "Optimal Geostationary Orbit Transfers Using Onboard Chemical-Electric Propulsion," *Journal of Spacecraft and Rockets*, Vol. 49, No. 6, 2012, pp. 1174–1182. https://doi.org/10.2514/1.A32213.

[14] Macdonald, M., and Owens, S. R., "Combined high and low-thrust geostationary orbit insertion with radiation constraint," *Acta Astronautica*, Vol. 142, 2018, pp. 1–9. https://doi.org/10.1016/j.actaastro.2017.10.011.

[15] Morante, D., Sanjurjo-Rivo, M., Soler, M., and Sánchez-Pérez, J. M., "Hybrid multi-objective orbit-raising optimization with operational constraints," *Acta Astronautica*, Vol. 175, 2020, pp. 447–461. https://doi.org/10.1016/j.actaastro.2020.05.022.

[16] Jenkin, A., "Representative Mission Trade Studies for Low-Thrust Transfers to Geosynchronous Orbit," *AIAA/AAS Astrodynamics Specialist Conference and Exhibit*, 2004, pp. 1–27. https://doi.org/10.2514/6.2004-5086.

[17] Ceccherini, S., Mani, K. V., and Topputo, F., "Combined System–Trajectory Design for Geostationary Orbit Platforms on Hybrid Transfer," *Journal of Spacecraft and Rockets*, Vol. 59, No. 2, 2022, pp. 448–466. https://doi.org/10.2514/1.A35012.

[18] Lee, S., and Hwang, I., "Hybrid High- and Low-Thrust Optimal Path Planning for Satellite Formation Flying," *AIAA Guidance, Navigation, and Control Conference*, 2012, pp. 1–13. https://doi.org/10.2514/6.2012-5046.

[19] Kluever, C. A., "Spacecraft optimization with combined chemical-electric propulsion," *Journal of Spacecraft and Rockets*, Vol. 32, No. 2, 1995, pp. 378–380. https://doi.org/10.2514/3.26623.

[20] Kluever, C. A., "Optimal Earth-Moon Trajectories Using Combined Chemical-Electric Propulsion," *Journal of Guidance, Control, and Dynamics*, Vol. 20, No. 2, 1997, pp. 253–258. https://doi.org/10.2514/2.4060.

[21] Cline, B. C., Parker, K. I., Rosales, J. J., Rovey, J. L., and West, S. T., "Lunar SmallSat Missions with Chemical-Electrospray Multimode Propulsion," *Journal of Spacecraft and Rockets (In review)*, 2023.

[22] Diprinzio, M., Edelman, P., Fruth, G., Guzman, J., Hartmann, J., Huang, R., Gearhart, J., Markin, R., Ranieri, C., and Lantukh, D., "AL YAH 3 Recovery and Orbit Transfer Design," *Proceedings of the AAS/AIAA Space Flight Mechanics Meeting*, Advances in the Astronautical Sciences, Vol. 168, Univelt, Inc., Ka'anapali, HI, 2018, pp. 179–198.

[23] Bryson, A. E., and Ho, Y.-C., *Applied Optimal Control: Optimization, Estimation, and Control*, 1st ed., Routledge, 1975. https://doi.org/10.1201/9781315137667.

[24] Karush, W., "Minima of functions of several variables with inequalities as side conditions," Ph.D. thesis, The University of Chicago, 1939. URL https://catalog.lib.uchicago.edu/vufind/Record/4111654.

[25] Kuhn, H. W., and Tucker, A. W., "Nonlinear Programming," *Proceedings of the Second Berkeley Symposium on Mathematical Statistics and Probability*, Vol. 2, University of California Press, 1951, pp. 481–493. URL https://projecteuclid.org/ebooks/berkeley-symposium-on-mathematical-statistics-and-probability/Proceedings-of-the-Second-Berkeley-Symposium-on-Mathematical-Statistics-and/chapter/Nonlinear-Programming/bsmsp/1200500249.

[26] Morante, D., Sanjurjo Rivo, M., and Soler, M., "A Survey on Low-Thrust Trajectory Optimization Approaches," *Aerospace*, Vol. 8, No. 3, 2021, pp. 1–39. https://doi.org/10.3390/aerospace8030088.

[27] Pascarella, A., Woollands, R., Pellegrini, E., Net, M. S., Xie, H., and Hook, J. V., "Low-thrust trajectory optimization for the solar system pony express," *Acta Astronautica*, Vol. 203, 2023, pp. 280–290. https://doi.org/10.1016/j.actaastro.2022.11.046.

[28] Pontryagin, L. S., *The mathematical theory of optimal processes*, English ed., Classics of Soviet Mathematics, Vol. 4, Gordon and Breach Science Publishers, New York, 1986.

[29] Betts, J. T., "Survey of Numerical Methods for Trajectory Optimization," *Journal of Guidance, Control, and Dynamics*, Vol. 21, No. 2, 1998, pp. 193–207. https://doi.org/10.2514/2.4231.

[30] Taheri, E., and Junkins, J. L., "Generic Smoothing for Optimal Bang-Off-Bang Spacecraft Maneuvers," *Journal of Guidance, Control, and Dynamics*, Vol. 41, No. 11, 2018, pp. 2470–2475. https://doi.org/10.2514/1.G003604.

[31] Taheri, E., Junkins, J. L., Kolmanovsky, I., and Girard, A., "A novel approach for optimal trajectory design with multiple operation modes of propulsion system, part 1," *Acta Astronautica*, Vol. 172, 2020, pp. 151–165. https://doi.org/10.1016/j.actaastro.2020.02.042.

[32] Taheri, E., Junkins, J. L., Kolmanovsky, I., and Girard, A., "A novel approach for optimal trajectory design with multiple operation modes of propulsion system, part 2," *Acta Astronautica*, Vol. 172, 2020, pp. 166–179. https://doi.org/10.1016/j.actaastro.2020.02.047.

[33] Taheri, E., "Composite Smooth Control Method for Low-Thrust Trajectory Design: Variable Specific Impulse Engine," *AIAA Scitech 2020 Forum*, 2020, pp. 1–17. https://doi.org/10.2514/6.2020-2184.

[34] Taheri, E., "Low-Thrust Trajectory Design Using Multi-Mode Propulsion Systems: A Grid-Based Thruster Model," *AIAA Scitech 2020 Forum*, 2020, pp. 1–18. https://doi.org/10.2514/6.2020-2183.

[35] Arya, V., Taheri, E., and Junkins, J. L., "Low-Thrust Gravity-Assist Trajectory Design Using Optimal Multimode Propulsion Models," *Journal of Guidance, Control, and Dynamics*, Vol. 44, No. 7, 2021, pp. 1280–1294. https://doi.org/10.2514/1.G005750.

[36] Arya, V., Taheri, E., and Junkins, J. L., "A composite framework for co-optimization of spacecraft trajectory and propulsion system," *Acta Astronautica*, Vol. 178, 2021, pp. 773–782. https://doi.org/10.1016/j.actaastro.2020.10.007.

[37] Woollands, R., and Taheri, E., "Optimal low-thrust gravity perturbed orbit transfers with shadow constraints," *Proceedings of the AAS/AIAA Astrodynamics Specialist Conference*, Advances in the Astronautical Sciences, Vol. 171, Univelt, Inc., Portland, ME, 2019, pp. 1303–1317.

[38] Quarta, A. A., and Mengali, G., "Minimum-time space missions with solar electric propulsion," *Aerospace Science and Technology*, Vol. 15, No. 5, 2011, pp. 381–392. https://doi.org/10.1016/j.ast.2010.09.003.

[39] Chi, Z., Li, H., Jiang, F., and Li, J., "Power-limited low-thrust trajectory optimization with operation point detection," *Astrophysics and Space Science*, Vol. 363, No. 6, 2018, p. 122. https://doi.org/10.1007/s10509-018-3344-8.

[40] Li, T., Wang, Z., and Zhang, Y., "Double-homotopy technique for fuel optimization of power-limited interplanetary trajectories," *Astrophysics and Space Science*, Vol. 364, No. 9, 2019, p. 144. https://doi.org/10.1007/s10509-019-3637-6.

[41] Lawden, D. F., *Optimal trajectories for space navigation*, Mathematical texts, Butterworth & Co., London, Butterworths, 1963.

[42] Prussing, J. E., *Optimal spacecraft trajectories*, first edition ed., Oxford University Press, Oxford, UK, 2018.

[43] Taheri, E., Kolmanovsky, I., and Atkins, E., "Enhanced smoothing technique for indirect optimization of minimum-Fuel low-Thrust trajectories," *Journal of Guidance, Control, and Dynamics*, Vol. 39, No. 11, 2016, pp. 2500–2511. https://doi.org/10.2514/1.G000379.

[44] Levenberg, K., "A Method For The Solution Of Certain Non-Linear Problems In Least Squares," *Quarterly of Applied Mathematics*, Vol. 2, No. 2, 1944, pp. 164–168. URL http://www.jstor.org/stable/43633451.

[45] Moré, J. J., "The Levenberg-Marquardt algorithm: Implementation and theory," *Numerical Analysis*, edited by G. A. Watson, Springer, Berlin, Heidelberg, 1978, pp. 105–116. https://doi.org/10.1007/BFb0067700.

[46] Verner, J. H., "Numerically optimal Runge–Kutta pairs with interpolants," *Numerical Algorithms*, Vol. 53, No. 2-3, 2010, pp. 383–396. https://doi.org/10.1007/s11075-009-9290-3.

[47] Dormand, J., and Prince, P., "A family of embedded Runge-Kutta formulae," *Journal of Computational and Applied Mathematics*, Vol. 6, No. 1, 1980, pp. 19–26. https://doi.org/10.1016/0771-050X(80)90013-3.

[48] Shampine, L. F., and Reichelt, M. W., "The MATLAB ODE Suite," *SIAM Journal on Scientific Computing*, Vol. 18, No. 1, 1997, pp. 1–22. https://doi.org/10.1137/S1064827594276424.

[49] Fisher, J., "NEXT-C Flight Ion System Status," *AIAA Propulsion and Energy Forum*, 2020, pp. 1–32. https://doi.org/10.2514/6.2020-3604.